Joint properties of friction welded joint between pure magnesium and pure aluminium with post-weld heat treatment

Masaaki KIMURA[a], Akiyoshi FUJI[b] and Shintaro SHIBATA[c]

a Department of Mechanical and System Engineering, Graduate School of Engineering, University of Hyogo, 2167 Shosha, Himeji, Hyogo, 671-2280 Japan
b Department of Mechanical Engineering, Faculty of Engineering, Kitami Institute of Technology, 165 Koen-cho, Kitami, Hokkaido, 090-8507 Japan
c Graduate student, Kitami Institute of Technology, 165 Koen-cho, Kitami, Hokkaido, 090-8507 Japan (Present Address: Sinfonia Technology Corporation Limited)

The present paper described the investigation of the joint properties of friction welded joint between pure magnesium (CP-Mg) and pure aluminium (CP-Al) with post-weld heat treatment (PWHT). The joint in as-welded condition fractured from the adjacent region of the weld interface, although that had the same strength as the tensile strength of the CP-Al base metal. This joint had the intermediate layer (interlayer) consisting of intermetallic compound (IMC) on the weld interface, and its thickness was below approximately 1 μm. Most of joints subjected to PWHT autogenously fractured at IMC interlayer and that mainly occurred between Mg_2Al_3 and $Mg_{17}Al_{12}$ although those layers had a little each other at the fractured surfaces. The IMC interlayer grew to CP-Mg and CP-Al sides, and its thickness increased with increasing heating temperature and/or heating time. The main reasons for the autogenous fracture from the adjacent region of the weld interface of the joint were considered the growth of IMC interlayer of the joint during PWHT process. Furthermore, that fracture of the joint was thought the generating of the thermal stresses in the radial and/or circumferential directions during the cooling stage of PWHT process.

Keywords: Magnesium, Aluminium, Friction welding, Post-weld heat treatment, Interlayer, Thermal stress

1. Introduction

Dissimilar metal joints (referred to as dissimilar joints) have some advantages such as high functionality characteristics for the industrial usage. Since an expansion in the use of dissimilar joints is expected and widely used in various component parts, easy welding method for dissimilar joints is strongly required. On the other hand, the dissimilar joints have several severe problems. In particular, one problem will occur when the dissimilar joints are operated at elevated temperature environment, and/or after post-weld heat treatment (referred to as PWHT). In addition, the intermediate layer (interlayer) consisting of a brittle intermetallic compound (IMC) will generate at the joint interface of both dissimilar metals, so that IMC interlayer will give fatal damage to equipments [1]. Some researchers had reported the mechanical and metallurgical properties of dissimilar joint, which was made with various welding method subjected to PWHT such as friction welding [2-4], friction stir welding [5-7], explosion welding [8], laser welding [9-11], electron beam welding [12,13], and arc welding [14-16]. However, even the PWHT condition of dissimilar joint made by friction welding method that has less generating IMC interlayer at the weld interface, has not been fully clarified. In particular, it is one of the main reasons for the concerned point that the joint will be fractured from the weld interface after PWHT [17,18]. To utilize of dissimilar joint for industrial usage, it is very essential to clarify the joint strength and fractured portion of that under various PWHT conditions, because it is considered that the joint will be used into high temperature conditions. Moreover, if the characteristics of dissimilar joint subjected to PWHT will be clarified, it will be also useful under extreme conditions such as aerospace industry.

In previous works, some of the authors were investigated as basic research that the effect of friction welding conditions on the mechanical (mainly tensile strength) and metallurgical properties of the joint with various PWHT conditions in addition to as-welded condition up to now for dissimilar joints made by friction welding method as following combinations: pure titanium (Ti) and austenitic stainless steel [19], pure Ti and pure aluminium (Al) [20], pure Ti and Al alloys [21], pure Ti and pure nickel (Ni) [22], Al alloys and low carbon steel (LCS) [23], pure Al and LCS [24], brass and LCS [25], and pure Al and pure Ni [26,27]. From those reports, even though the friction welding process can minimize the generation of IMC interlayer between dissimilar metals, it was estimated that IMC interlayer will be affected to PWHT condition for the joint fracture. In particular, it is very useful to clarify the fractured portion of dissimilar joint and that reason to design of the joint. However, the fractured portion of dissimilar joint differs, since mechanical properties such as the tensile strength and thermal properties such as the thermal conductivity are different in their combinations. Hence, to clarify the cause of the fractured portion of dissimilar joint subjected to PWHT is strongly required for design of the joint made by friction welding method, because the guideline of that joint for using into high

temperature condition will be obtained.

According to the back ground described above, the authors have been carrying out research to clarify the fracture mechanism of dissimilar joint made by friction welding method subjected to PWHT. In this report, the authors chose in the present work the combination of between pure magnesium (Mg) and pure Al, because an expansion in the use of those materials are expected in various component parts, and the joint of those combination will be expected to be used in the transport industry. Furthermore, this dissimilar joint in as-welded condition for those material combinations had IMC interlayer at the weld interface which will be described later. Hence, the authors investigate the fracture of the friction welded joint between pure Mg and pure Al, under various PWHT conditions, and also will clarify the composition of IMC interlayer and its growth mechanism, because it will be considered that the interlayer will grow during PWHT process. In addition, the authors will present about how the fracture will occur at the adjacent region of the weld interface of friction welded joint between pure Mg and pure Al during the cooling stage of PWHT process.

2. Experimental procedure

2.1 Materials and friction welding condition

Commercially pure Mg (referred to as CP-Mg) and commercially pure Al (referred to as CP-Al) of 16 mm diameter round bars were used throughout in the experiments in this study. CP-Mg bar had the chemical compositions of 0.006Al-0.01Mn-0.01Si-0.004Fe-Mg in balance (mass%), and that was supplied with an ultimate tensile strength of 219 MPa and an elongation of 8.0%, respectively. CP-Al bar had the chemical compositions of 0.25Si-0.40Fe-0.05Cu-0.05Mn-0.05Mg-0.05Zn-0.03Ti-Al in balance (mass%), and that was supplied with an ultimate tensile strength of 82 MPa, a 0.2% yield strength of 44 MPa, and an elongation of 42.5%, respectively. Both round bars were used for the experiments in this study as received condition. Those materials were machined to 70 mm length, i.e. the diameter of the weld faying (contacting) surface was 16 mm. Then, all weld faying surfaces were polished with a buff before joining in order to minimize the effect of its surface roughness on the joint properties [21].

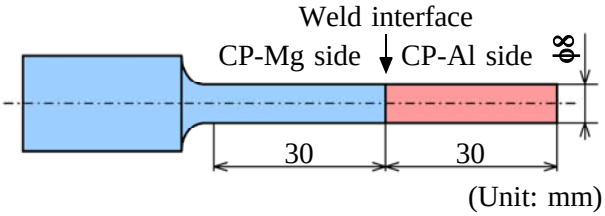

Fig. 1 Dimension of joint for fracture test during PWHT.

A continuous (direct) drive friction welding machine was employed for joining. During friction welding operations, the friction welding condition was set to the following combinations: a friction speed of 25 s^{-1} (1500 rpm), a range of friction pressures from 10 to 50 MPa, a range of friction times from 0.5 to 2.5 s, a forge pressure of 90 MPa, and a forge time of more than 6.0 s. All joint tensile test specimens were machined to 12.5 mm diameters and 60 mm in parallel length. Then, the joint tensile test was carried out in as-welded condition (hereafter the joint with this condition called as the AW joint) at room temperature. In addition, analysis via SEM-EDS was carried out to analyse the chemical composition at the adjacent region of the weld interface for the joint in as-welded condition.

2.2 Fracture test of joint and PWHT condition

The fracture test of joint subjected to PWHT was carried out as follows. The specimen for the fracture test was machined to 8 mm in diameter in parallel length as shown in Fig. 1, and it was machined to AW joint. Figure 2 shows the fracture test equipment with a vacuum furnace that carried out with PWHT in order to progress with IMC interlayer growth. The joint (the specimen for the fracture test) was set on the spacer that was put into a vacuum furnace, CP-Mg side of its joint was set to like as a cantilever. Furthermore, two kinds of thermocouples were attached to CP-Mg and CP-Al sides respectively, for the fracture test. One thermocouple was used for measuring temperature of the joint, and another was for measuring occurrence of

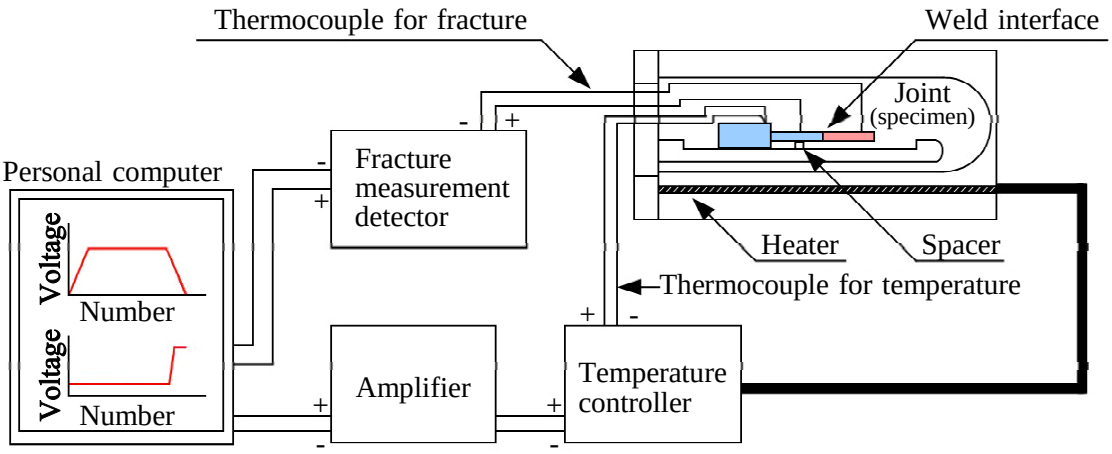

Fig. 2 Schematic illustration of joint fracture test equipment.

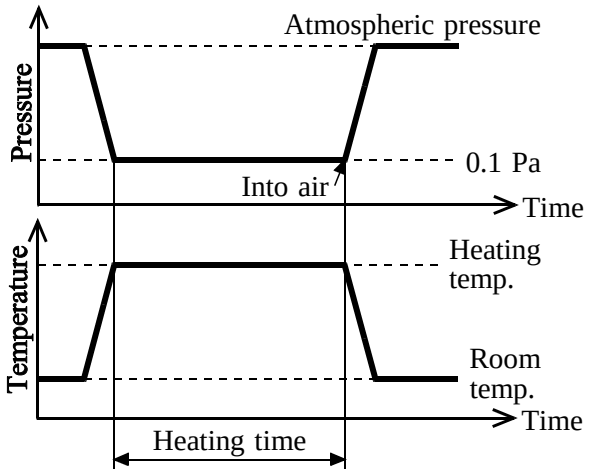

Fig. 3 Pressure and temperature cycle diagrams of PWHT.

fracture for it during this process. The former thermocouple was connected to the large diameter part of the joint (CP-Mg side), and the latter one was connected to the 8 mm diameter part of that (CP-Al side). When the joint fractured from the adjacent region of the weld interface during PWHT, the latter thermocouple indicated its temperature and timing with a breaking of measuring current. Figure 3 shows the pressure and temperature cycle diagrams of PWHT. The heating temperatures were at 423 to 673 K (150 to 400 ℃) and the heating times were from 43.2 to 86.4 ks (12 to 24 hours), and those were set under the vacuum environment of approximately 0.1 Pa (7.5×10^{-4} torr), which was shown in Fig. 3. Then, when PWHT to the joint was finished with a setting heating time, it was cooled to room temperature by furnace cooling, i.e. the heating was stopped. Thereafter, this joint (hereafter the joint with this condition called as the PWHT joint) was taken out from the furnace. The details of this experimental method were the same of those in a previous report [26]. After fracture test, analysis via SEM-EDS was carried out to analyse the chemical composition at the cross-section of PWHT joint. In this case, some samples for SEM observation of the cross-sections of PWHT joints were mounted into resin for ease of handling, and those were analysed. Furthermore, the fractured surfaces of PWHT joints were also analysed using X-ray diffraction analysis.

2.3 *In situ* observation of IMC interlayer of joint

To clarify the characteristics of the IMC interlayer of the joint, the continuous *in situ* observation during PWHT process was carried out. The specimen (AW joint) was used with the shape wherein the adjacent region of the weld interface of the joint was processed with 3 mm in diameter and 3 mm in thickness by wire electric discharge machining. Then, the continuous *in situ* observation during PWHT process was carried out at a heating temperature of 573 (300 ℃) and/or 673 K, and it was heat treated in a vacuum environment. A high temperature microscope was used for the observation of the IMC interlayer growth at the weld

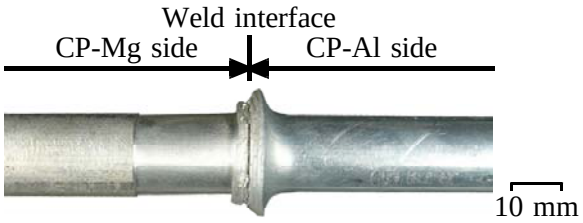

Fig. 4 Example of joint appearance; friction time of 50 MPa and friction time of 1.0 s.

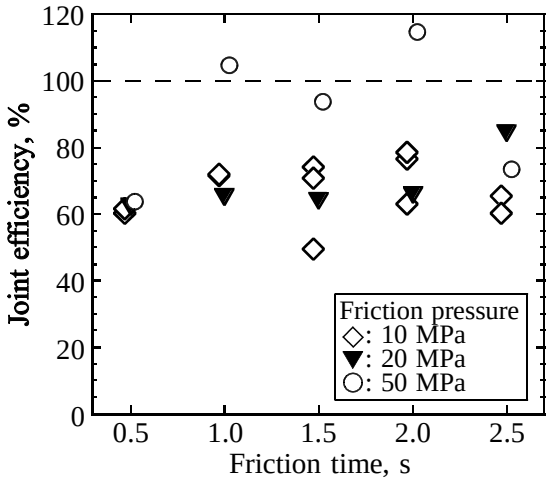

Fig. 5 Relationship between friction time and joint efficiency of AW joint.

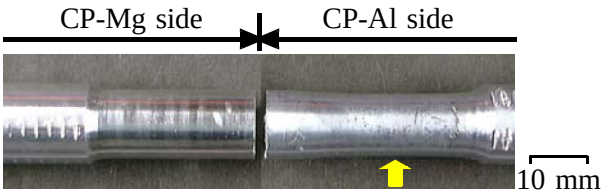

Fig. 6 Example of appearance of joint tensile tested specimen for AW joint.

interface, which was recorded continuously using digital video. The detailed method of this *in situ* observation has been described in previous reports [20,24].

3. Results

3.1 Properties of as-welded joint

To clarify the characteristics of AW joint, the tensile and metallurgical properties of that was investigated. Figure 4 shows an example of the joint appearance at a friction time of 50 MPa and a friction time of 1.0 s. The flash (burr or collar) of CP-Mg and CP-Al was exhausted from the weld interface. That is, the appearance of AW joint was displayed as completely joined, although the quantities of the flash differed at the joint with other friction welding conditions. Figure 5 shows the relationship between the friction time and the joint efficiency of AW joint. The joint efficiency was defined as the ratio of joint tensile strength to the ultimate tensile strength of the CP-Al base metal. Figure 6 shows an example of the appearance of the joint tensile tested specimen for AW joint. When the joint was made with a friction pressure of 10 MPa as showed by the open rhombus symbols in Fig. 5, the joint

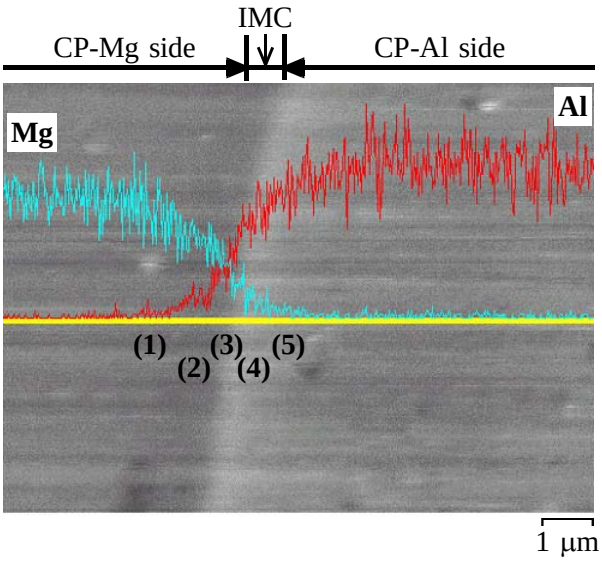

Located portion	Chemical composition, mol.%	
	Mg	Al
(1)	91.1	8.9
(2)	74.4	25.6
(3)	44.0	56.0
(4)	7.5	92.5
(5)	1.0	99.0

Fig. 7 SEM image and EDS analysis result at central portion on adjacent region of weld interface for cross-section of AW joint; friction pressure of 50 MPa and friction time of 1.0 s.

efficiency was approximately 60% at a friction time of 0.5 s. The joint efficiency at other friction times was also around 60% although that had a scattering. In addition, the joint efficiency with a friction pressure of 20 MPa as showed by the solid inverted triangle symbols was approximately 60%. That is, the joint efficiency of AW joint with a friction pressure of 10 MPa was kept around 60% regardless of friction time. On the other hand, when the joint was made with a friction pressure of 50 MPa as showed by the open circular symbols, the joint efficiency was around 100% at friction times of 1.0 to 2.0 s. That is, the joint with high friction pressure and opportune friction time had high tensile strength that was similar to the tensile strength of CP-Al base metal. However, all joints fractured at the adjacent region of the weld interface as shown in Fig. 6, although those joints with around 100% joint efficiency had the plastic deformation on the CP-Al side which was indicated by an arrow in this figure. In this case, the joint efficiency of some joints was obtained 100% or higher, because the parallel part length of the joint tensile test specimen was shorter. The IMC interlayer at the weld interface of the joint affected to the tensile strength of its joint, and that was also reported by some authors although the friction welding conditions differed [28-30].

Figure 7 shows the SEM image and EDS analysis result at the central portion on the adjacent region of the

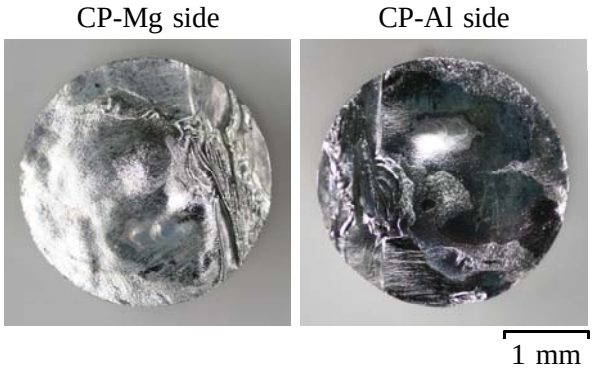

Fig. 8 Example of fractured surfaces of PWHT joint.

weld interface for the cross-section of AW joint. This joint was made with a friction pressure of 50 MPa and a friction time of 1.0 s. The distribution lines corresponding to Mg and Al had a slightly plateau part at the weld interface, although the weld interface was slightly unclear. The chemical composition of the location (1) was 91.1%Mg-8.9%Al (in mol.%). It was considered that this location was CP-Mg side. The composition of the location (2) was 74.4%Mg-25.6%Al and this part will be considered as the transition area. Those of locations (4) and (5) were 7.5%Mg-92.5%Al and 1.0%Mg-99.0%Al, respectively. It was considered that those locations were CP-Al side although those had scattering. On the other hand, the composition of the location (3) was 44.0%Mg-56.0%Al. That is, it was considered that the location (3) was the IMC interlayer. However, it was difficult to identify the IMC interlayer based on the SEM observation level because that thickness was very thin such as below 1 μm, and the peak was unclear by X-ray diffraction analysis. Therefore, although further investigation will be needed to establish the friction welding condition for obtaining the joint without IMC interlayer at the weld interface, that interlayer seems to be the cause of the fracture of AW joint from the adjacent region of the weld interface as shown in Fig. 6. In addition, it was clarified that the joint fractured portion was affected to IMC interlayer, of which thickness was below 1 μm, although the joint had 100% joint efficiency. The similar IMC interlayer was also observed in some dissimilar joints in other welding method such as diffusion welding [31], friction stir welding [32], friction stir spot welding [33], ultrasonic welding [34], explosion welding [35], laser welding [36], and roll welding [37].

3.2 Properties of PWHT joint

To clarify the effect of the joint properties on IMC interlayer at the weld interface of AW joint, PWHT was carried out to that joint. However, when the joint (PWHT joint) took out from a vacuum furnace, almost all joints already fractured from the adjacent region of the weld interface as shown in Fig. 6, although it did not have the plastic deformation on the CP-Al side. That is, the joint autogenously fractured during PWHT process. Furthermore, the PWHT joint with low heating temperature of below 623 K (350 ℃) did not have the

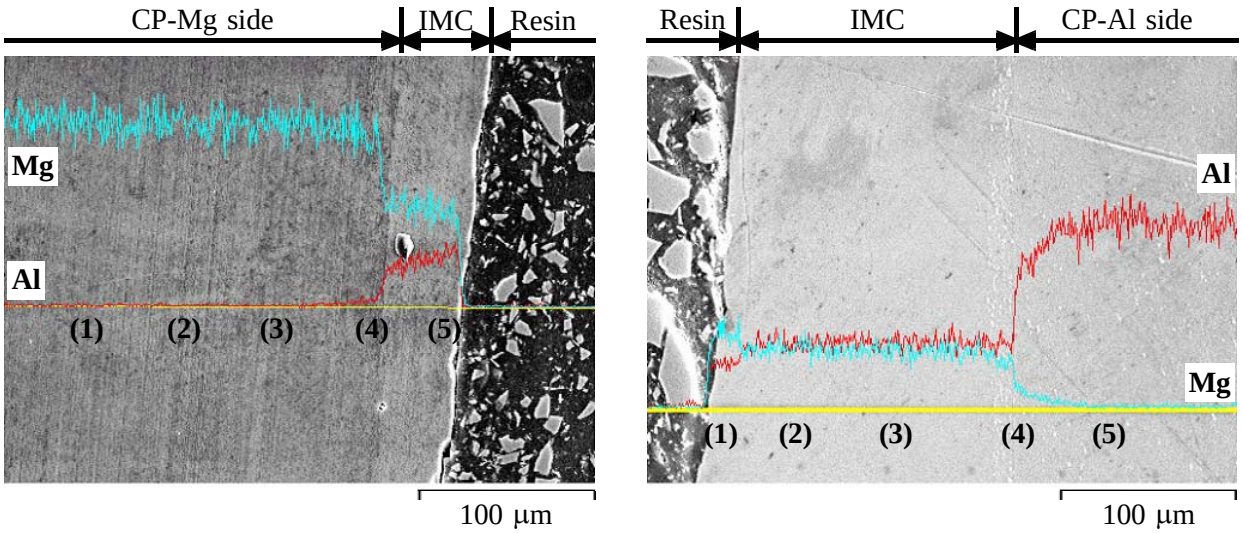

Located portion	Chemical composition, mol.%	
	Mg	Al
(1)	100.0	0.0
(2)	100.0	0.0
(3)	100.0	0.0
(4)	94.8	5.2
(5)	49.5	50.5

(a) CP-Mg side

Located portion	Chemical composition, mol.%	
	Mg	Al
(1)	46.8	53.2
(2)	36.2	63.8
(3)	37.1	62.9
(4)	2.2	97.8
(5)	1.3	98.7

(b) CP-Al side

Fig. 9 SEM images and EDS analysis results at central portion on adjacent region of weld interface for cross-section of PWHT joint; heating temperature of 673 K and heating time of 86.4 ks.

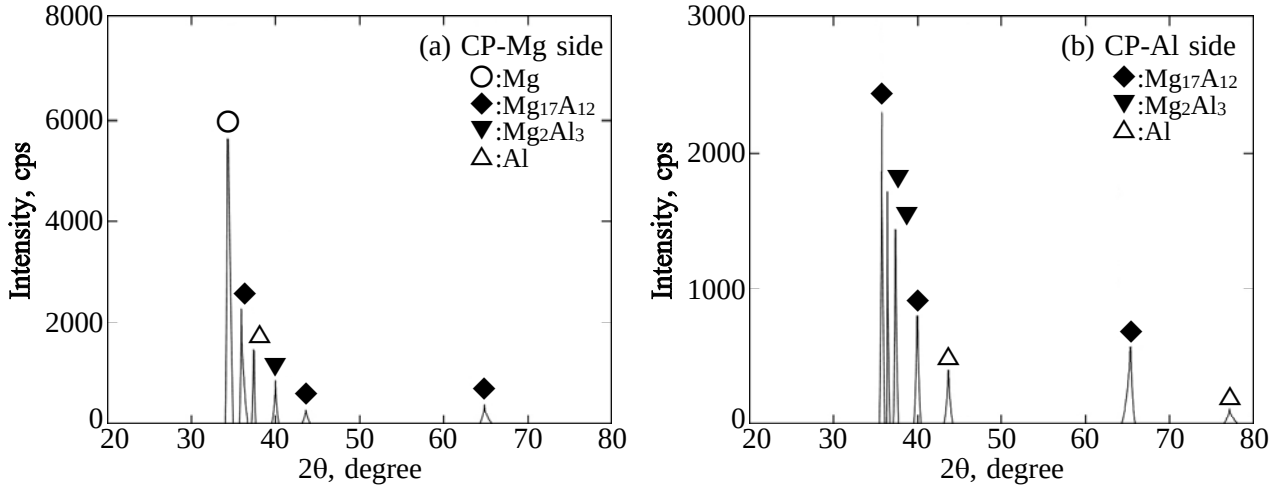

(a) CP-Mg side (b) CP-Al side

Fig. 10 X-ray diffraction analysis results of fractured surfaces of PWHT joint; heating temperature of 673 K and heating time of 86.4 ks.

autogenous fracture, but that had the fracture at the adjacent region of the weld interface (data not shown due to space limitations). In brief, all PWHT joints fractured at the adjacent region of the weld interface through PWHT. Figure 8 shows an example of the fractured surfaces of joint fracture test specimen after PWHT. This joint was made with a friction pressure of 50 MPa and a friction time of 1.0 s, and it was treated with a heating temperature of 673 K and a heating time of 43.2 ks, i.e. it had the autogenous fracture during PWHT process. The fractured surfaces showed an almost flat face, i.e. the PWHT joint had a brittle fracture. Hence, it was considered that the generating and growing of IMC interlayer seems to be the cause of the autogenous fracture of the joint, because AW joint had also the interlayer at the weld interface (see Fig. 7).

Figure 9 shows the SEM images and EDS analysis results at the central portion on the adjacent region of the weld interface for the cross-section of PWHT joint. This PWHT joint was treated with a heating

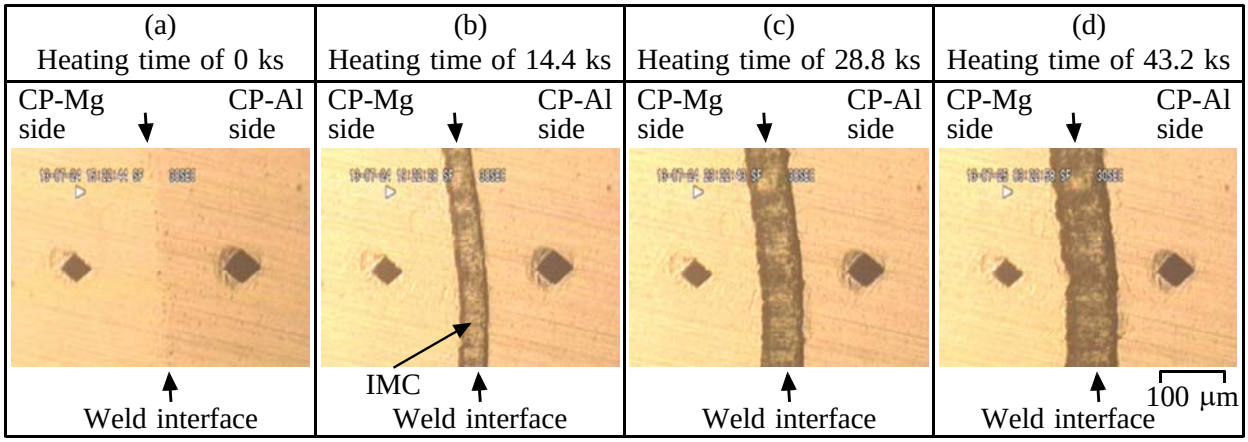

Fig. 11 Microstructures at central portion on adjacent region of weld interface for cross-section of AW joint during PWHT; heating temperature of 673 K.

temperature of 673 K and a heating time of 86.4 ks. The distribution lines corresponding to Mg and Al had a plateau part at the weld interface of the CP-Mg side as shown in Fig. 9a. The compositions of the locations (1) to (3) were 100%Mg, and that of the location (4) was 94.8%Mg-5.2%Al, respectively. It was considered that those locations were CP-Mg side, although it had scattering. However, the composition of the location (5) was 49.5%Mg-50.5%Al. That is, the location (5) was the IMC interlayer, and its width was approximately 46 μm. It was considered that this interlayer was $Mg_{17}Al_{12}$. The composition of this location was similar to that of AW joint (see Fig. 7). On the other hand, the distribution lines had also a plateau part at the weld interface of the CP-Al side, as shown in Fig. 9b. The composition of the location (1) was 46.8%Mg-53.2%Al, and then that at (2) and (3) were (36.2-37.1)%Mg-(62.9-63.8)%Al, respectively. Those locations were the IMC interlayer, and its width was approximately 173 μm. That is, the chemical composition of the location (1) differed with that of locations (2) and (3). Therefore, it was considered that the IMC interlayer composed two layers. In addition, it was considered that the IMC interlayer of the location (1) was $Mg_{17}Al_{12}$ and that at locations (2) and (3) was Mg_2Al_3, respectively. The compositions of locations (4) and (5) were (1.3-2.2)%Mg-(97.8-98.7)%Al, and it was considered that those were CP-Al side. The joint with other PWHT conditions as well as the other observed portion in this PWHT joint had two layers at the weld interface, although those results were not shown here. Hence, it was clarified that the joint had the autogenous fracture by the growth of IMC interlayer.

Figure 10 shows the X-ray diffraction analysis results of the fractured surfaces on CP-Mg and CP-Al sides of PWHT joint, respectively. In this case, PWHT joint was also treated with a heating temperature of 673 K and a heating time of 86.4 ks. Mainly $Mg_{17}Al_{12}$ and Mg_2Al_3 diffraction patterns were detected on the CP-Mg side fractured surface as well as Mg and Al was detected on it (Fig. 10a). In addition, mainly $Mg_{17}Al_{12}$ and Mg_2Al_3 diffraction patterns were detected on the CP-Al side fractured surface as well as Al was detected on it (Fig. 10b). That is, both fractured surfaces had $Mg_{17}Al_{12}$ and Mg_2Al_3, and the IMC interlayer of the PWHT joint was composed with those layers. Therefore, it was clarified that the joint had the autogenous fracture from between $Mg_{17}Al_{12}$ and Mg_2Al_3 layers.

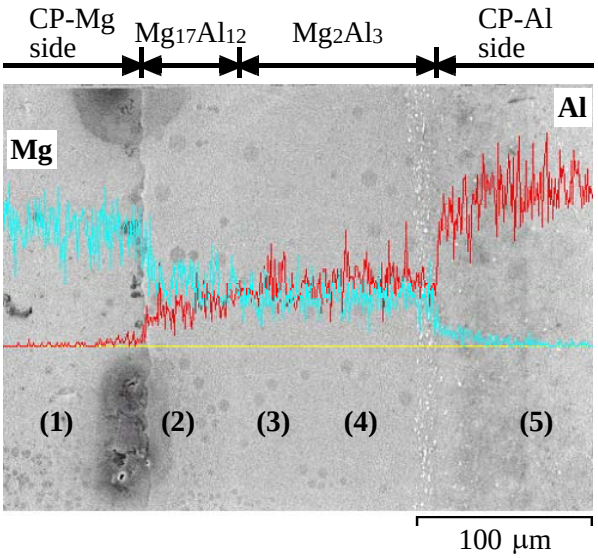

Located portion	Chemical composition, mol.%	
	Mg	Al
(1)	100.0	0.0
(2)	46.6	53.4
(3)	34.8	65.2
(4)	33.2	66.8
(5)	0.0	100.0

Fig. 12 SEM image and EDS analysis result at central portion on adjacent region of weld interface for cross-section of AW joint through PWHT; heating temperature of 673 K and heating time of 43.2 ks.

3.3 *In site* observation of IMC interlayer

Figure 11 shows the microstructures at the central portion on the adjacent region of the weld interface for the cross-section of AW joint during PWHT process. In

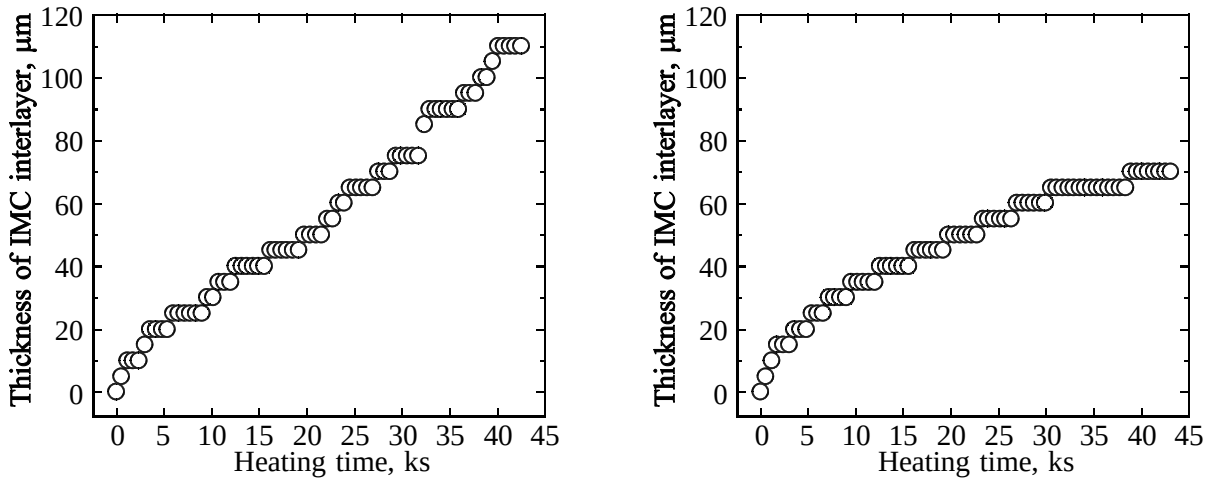

(a) Heating temperature of 673 K (b) Heating temperature of 573 K

Fig. 13 Relationship between heating time and thickness of IMC interlayer at central portion of weld interface for AW joint during PWHT at various heating temperatures.

this case, a heating temperature was set to 673 K. In addition, the region for *in site* observation had the indentation marks produced by Vickers hardness test machine to clarify the generating and growing of IMC interlayer. The IMC interlayer was not observed at the weld interface of AW joint as shown in Fig. 11a, because that interlayer was very thin as shown in Fig. 7. However, the IMC interlayer grew toward CP-Mg and CP-Al sides, and its thickness was increased with increasing heating temperature (see Figs. 11b through 11d). That is, the IMC interlayer grew with increasing heating time. The growth of IMC interlayer was observed in other heating temperatures, although those results were not shown here. In this connection, the growth of IMC interlayer was also reported of other welding technique [38,39], although those were not *in site* observation results.

Figure 12 shows the SEM image and EDS analysis result at the central portion on the adjacent region of the weld interface for the cross-section of AW joint through PWHT with a heating temperature of 673 K and a heating time of 43.2 ks. The IMC interlayer was observed clearly, and its width was approximately 147 μm. The composition of the location (1) was 100%Mg, and that at (6) was 100%Al, respectively. Those locations were each base metals. The composition of the location (2) was 46.6%Mg-53.4%Al, and it was $Mg_{17}Al_{12}$. The compositions of the locations (3) and (4) were (33.2-34.8)%Mg-(65.2-66.8)%Al, and it was Mg_3Al_2. The compositions of those interlayers of AW joint by *in site* observation, which was treated with PWHT, corresponded to that of PWHT joint. Hence, AW joint had IMC interlayer through PWHT, of which composed with $Mg_{17}Al_{12}$ and Mg_3Al_2.

Figure 13 shows the relationship between heating time and thickness of IMC interlayer at the central portion of the weld interface for AW joint during PWHT process at various heating temperatures. The data in Fig. 13 were measured from the recorded digital video camera by *in site* observation as shown in Fig. 11. When AW joint was heat treated at a heating temperature of 673 K as shown in Fig. 13a, the thickness of IMC interlayer increased with increasing heating time. In addition, the thickness of IMC interlayer increased with increasing heating time at a heating temperature of 573 K as shown in Fig. 13b. However, the growth percentage of IMC interlayer by heating time differed. That is, the thickness of IMC interlayer at a heating temperature of 673 K was thicker than that of 573 K. Hence, the IMC interlayer grew by increasing heating temperature and/or heating time, and it was clarified. This autogenous fracture of the joint was the same result of that between pure Ni and pure Al [26].

4. Discussion

Based on the above results, the joint between CP-Mg and CP-Al had the IMC interlayer, which was mainly composed of $Mg_{17}Al_{12}$ and Mg_2Al_3, at the weld interface, and those layers grew by increasing heating temperature and/or heating time. Furthermore, this joint had the autogenous fracture from between those layers by PWHT (see Figs. 8 and 9). To clarify the autogenous fracture of the joint during PWHT process, the calculation of the thermal stress at the adjacent region of the weld interface of the joint by thermal elastic-plastic analysis with the finite element method (FEM) method were carried out.

4.1 Calculation method for thermal analysis of joint during PWHT process

FEM analysis program was developed by some of the authors, which used FORTRAN in order to elucidate the thermal stress distribution at the adjacent region of the weld interface of the joint during the cooling stage of PWHT process. FEM model, i.e. the directions of stresses and its mesh design are illustrated in Fig. 14. The dimensions of the model were determined, and that corresponded to the experimental result of the investigation for the properties of PWHT joint (see

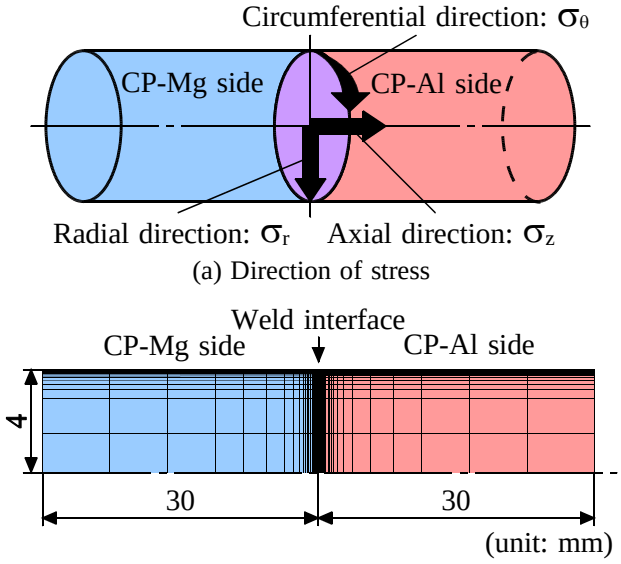

Fig. 14 Calculation model of thermal stress at adjacent region of weld interface for joint by thermal elastic-plastic analysis.

section 3.2). The directions of thermal stresses for the calculation were the radial, circumferential, and axial (longitudinal) directions, and those were shown in Fig. 14a. Also, this model had an axi-symmetric body, and the mesh size of the adjacent region of the weld interface was smaller than that of another region, because the residual stress at the adjacent region of the interface of dissimilar joint was affected by the mesh size [40], as shown in Fig. 14b. In this case, the IMC interlayer was not considered because to clarify the effect of the properties of welding materials. Then, the calculation for the thermal elastic-plastic analysis was carried out. The materials properties such as tensile strength [41-43], yield strength [41-43], Young's modulus [43-45], Poisson's ratio [44,45], and thermal expansion coefficient [43,46,47] of both base metals depend on temperature, and those were used for calculation, and those were summarized in Figs. 15a to 15e. By the way, one of the purposes of this study was to clarify the effect of thermal stress incited by PWHT for the joint fracture. Therefore, the initial stresses (e.g. residual stress) in the radial and circumferential directions of AW joint was not considered, i.e. the thermal elastic-plastic analysis of AW joint during the friction and forge processes was not carried out in actual calculation. In this connection, the residual stress of many dissimilar joints will be relaxed by PWHT [40]. That is, the generated residual stress at the adjacent region of the weld interface of the joint after welding (AW joint) is reduced during PWHT process since the soft material side of dissimilar joint is relaxed. However, it was reported that some joints was not necessarily reduced through PWHT [48,49], because new thermal stress is generated during the cooling stage of PWHT process. Hence, the residual stress of AW joint could be considered being negligible in this study, and the calculation of the thermal stress of the joint during the friction process at the welding was not carried out because the target for this study was clarification of the fracture mechanism for the dissimilar joint during PWHT process. Therefore, the element was assumed to be uniformly subjected to the temperature change during the cooling stage of PWHT process. In addition, the axial direction and the fixed ends of the CP-Mg and CP-Al sides were restrained. The details of the mesh design and calculation method were similar to those in a previous report [27]. In this connection, the calculated thermal stress at the outer surface was not considered, because the singular point of thermal stress occurred at this portion [27,50].

4.2 Thermal stress of joint subjected to PWHT

Figure 16 shows examples of the analytical results of the thermal stress in the axial direction of the joint subjected to PWHT. In this case, Fig. 16a showed the stress distribution across the weld interface at room temperature, Fig. 16b showed the stress distribution of the radial direction on the weld interface at room temperature, and Fig. 16c showed the relationship between cooling temperature during PWHT process and stress, respectively. Also, the tension of the thermal stress was shown as the plus (+), and the compression of that was shown as the minus (-), respectively. The joint at room temperature after PWHT had large thermal stress across the weld interface below about 13.2 mm (about 6.6 mm on each side), as shown in Fig. 16a. The maximum thermal stress was -59.8 MPa at the distance from the weld interface of 0.35 mm in the CP-Mg side, and that was +28.4 MPa at 0.9 mm in the CP-Al side, respectively. In addition, the thermal stress at the axial centre portion was smaller than that of the adjacent region of the outer surface (outer surface portion), as shown in Fig. 16b. The maximum stress at the outer surface portion was obtained -12.8 MPa at the distance from the axial centre of 3.945 mm in the CP-Mg side and -9.8 MPa at 3.945 mm in the CP-Al side, respectively. Moreover, the thermal stress was generated at a cooling temperature below 613 K (340 ℃) during PWHT process, and the maximum stress was obtained at room temperature after PWHT, as shown in Fig. 16c. That is, those results were meaning that the joint was generating thermal stress in the axial direction through the cooling stage until room temperature during PWHT process. Hence, it was considered that the thermal stress in the axial direction of the joint subjected to PWHT will be affected to the joint fracture from the adjacent region of the weld interface.

Figure 17 shows those results in the radial direction. The joint at room temperature had also large thermal stress across the weld interface below about 13.2 mm, as shown in Fig. 17a. The maximum thermal stress was +82.3 MPa at the distance from the weld interface of 0.05 mm in the CP-Mg side, and that was -60.8 MPa at 0.05 mm in the CP-Al side, respectively. The direction of the thermal stresses differed with the result of Fig. 16a. In addition, the thermal stress at the axial centre portion was larger than that of the outer surface portion,

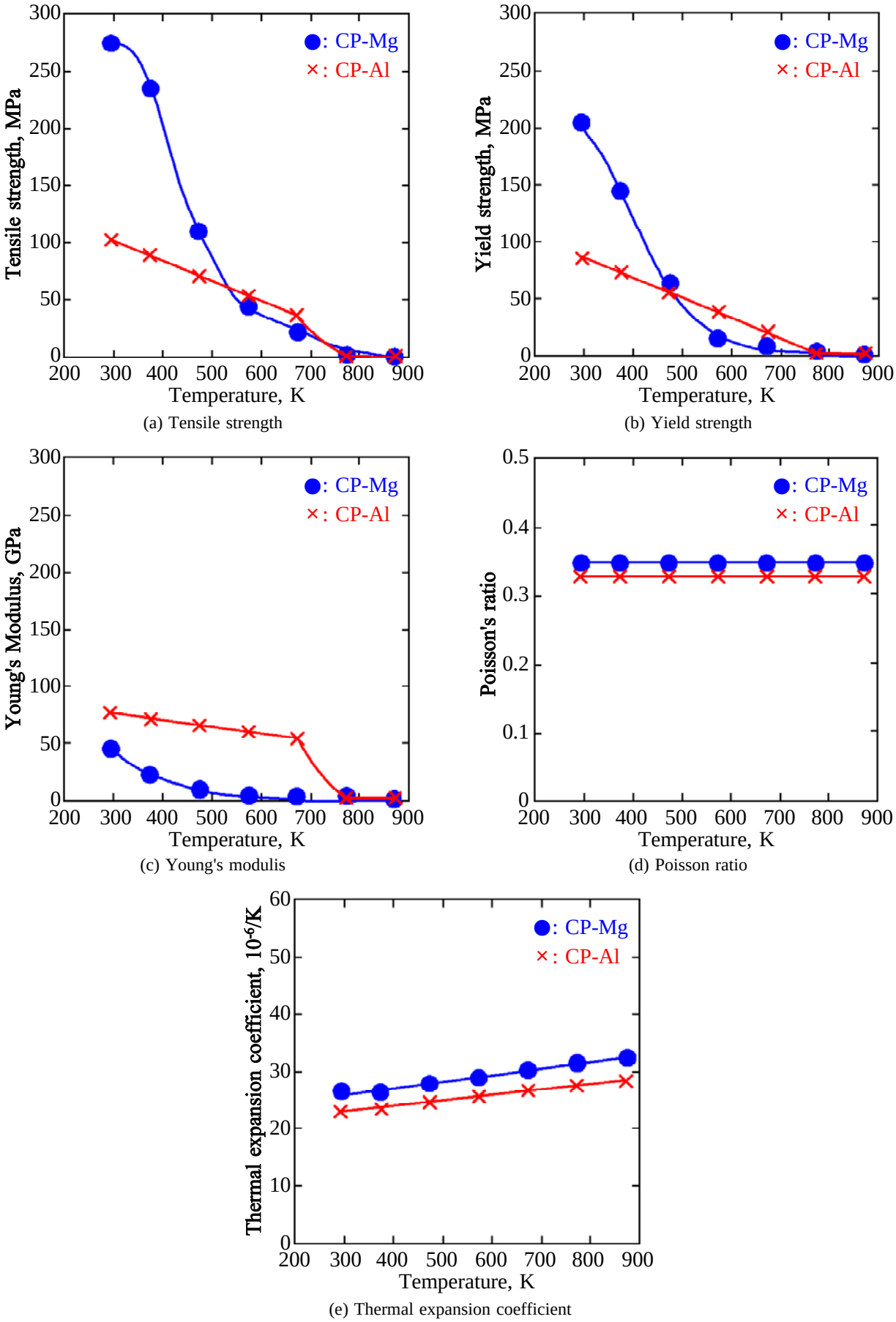

Fig. 15 Materials properties of CP-Mg and CP-Al base metals.

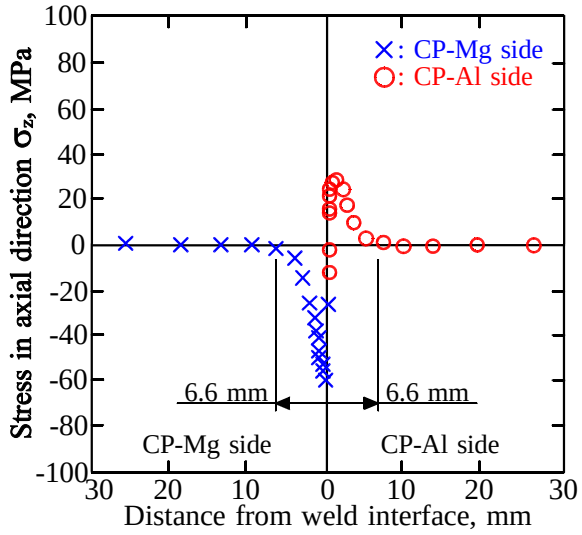

(a) Stress distribution across weld interface region at room temperature

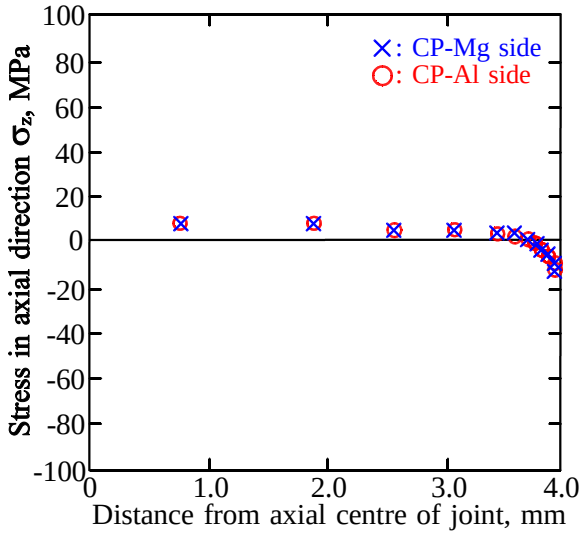

(b) Stress distribution of radial direction on weld interface at room temperature

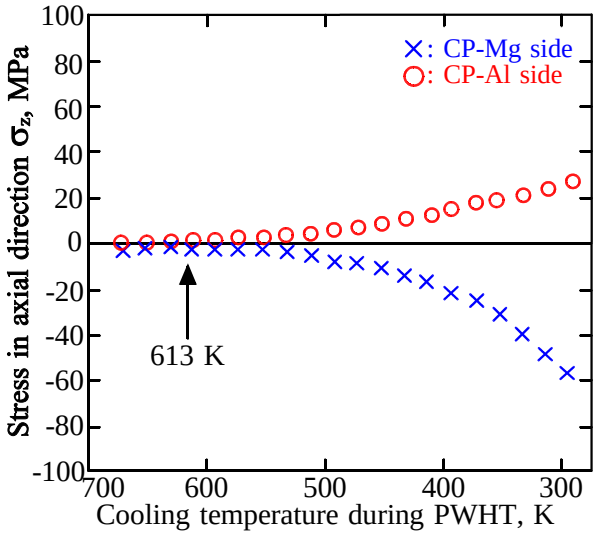

(c) Relationship between cooling temperature during PWHT and stress

Fig. 16 Examples of analytical results of stress in axial direction of joint subjected to PWHT.

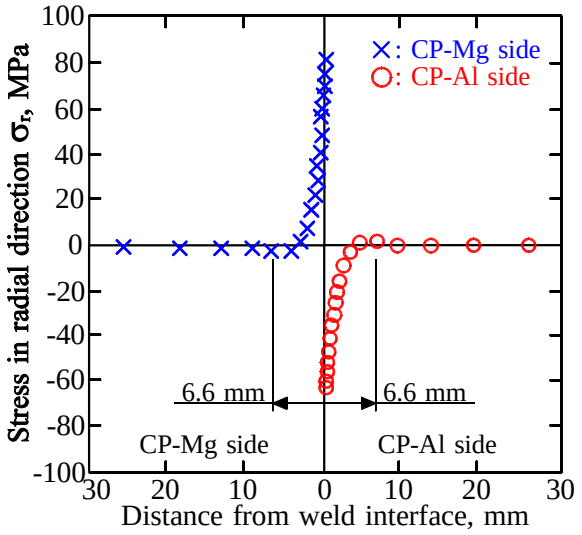

(a) Stress distribution across weld interface region at room temperature

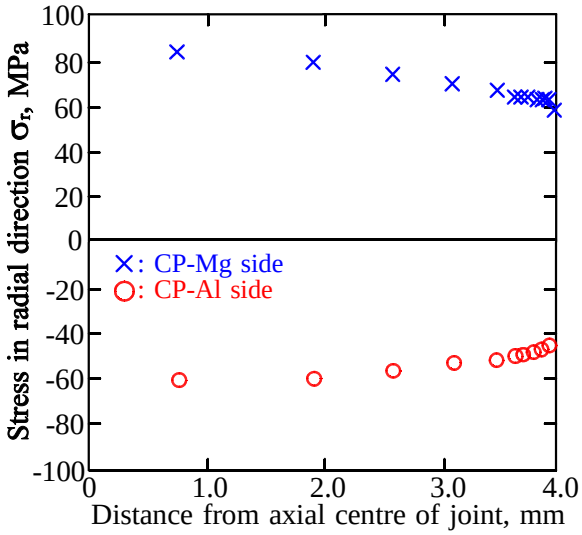

(b) Stress distribution of radial direction on weld interface at room temperature

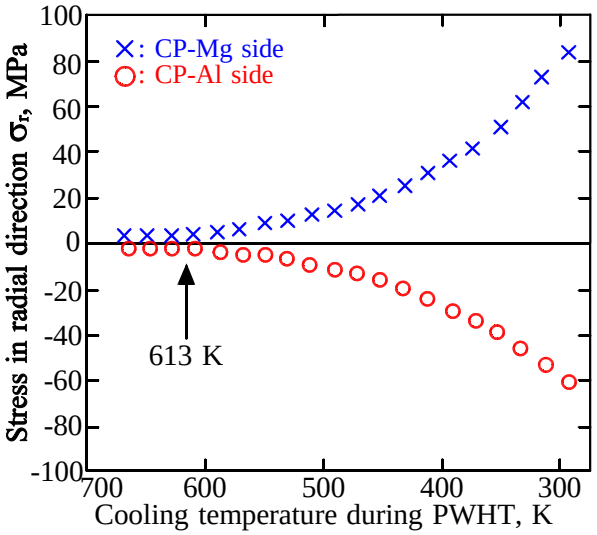

(c) Relationship between cooling temperature during PWHT and stress

Fig. 17 Examples of analytical results of stress in radial direction of joint subjected to PWHT.

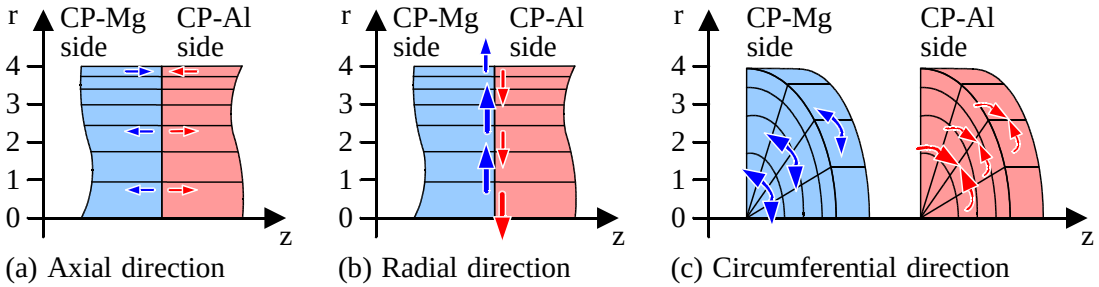

Fig. 18 Summarized schematic illustrations of analytical results of thermal stress in axial, radial, and circumferential directions of joint at room temperature after PWHT.

as shown in Fig. 17b. The maximum stress at the outer surface portion was obtained +82.3 MPa at the distance from the axial centre of 0.75 mm in the CP-Mg side, and -60.8 MPa at 0.75 mm in the CP-Al side, respectively. The thermal stress was also generated at a cooling temperature below 613 K during PWHT process, and the maximum stress was obtained at room temperature after PWHT, as shown in Fig. 17c. Furthermore, the results in the circumferential direction were similar to that of the radial direction, and this analysis was axi-symmetric thermal elastic-plastic analysis in this study, so that the stress of the radial direction was theoretically equal to that of the circumferential direction at the centre axis (axial centre) of the joint [27]. Hence, those results were meaning that the joint was generating thermal stress in the radial direction through the cooling stage until room temperature during PWHT process. Therefore, the thermal stress in the radial direction of the joint subjected to PWHT will be also affected to the joint fracture from the adjacent region of the weld interface.

Figure 18 summarized the schematic illustrations of the analytical results of the thermal stress in the axial, radial, and circumferential directions of the joint at room temperature after PWHT. The typical portions along the axial direction, i.e. the axial centre, half-radius, and peripheral portions are illustrated. In addition, the arrow direction indicates the stress direction. The thermal stress in the axial direction of the outer surface portion at room temperature was compression and the others were tension, as shown in Fig. 18a. However, the tension thermal stresses of those portions were smaller than the compression thermal stress of the outer surface portion (see Fig. 16). Hence, it was considered that those tension thermal stresses were not affected to the joint fracture. On the other hand, the thermal stress in the radial direction of the CP-Mg side was tension, and that of the CP-Al side was compression, as shown in Fig. 18b. The thermal stress in the circumferential direction of the CP-Mg side was tension, and that of the CP-Al side was compression as shown in Fig. 18b. Hence, those thermal stresses were affected to the joint fracture. Furthermore, those thermal stresses were obtained at room temperature. That is, the thermal stresses in the radial and circumferential directions were generated at a cooling temperature below 613 K during PWHT process and the maximum values were obtained at room temperature after PWHT (see Figs. 16c and 17c). Of course, it is necessary to clarify the physical meaning of this temperature. However, it will be estimated that the joint did not have the autogenous fracture with high temperature environment (during PWHT) by the thermal stress, and that occurred through the cooling stage until room temperature during PWHT process. It was considered that the joint will be autogenously fractured by the thermal stress mainly generated at the radius and/or circumferential directions during the cooling stage of PWHT process, although further investigation is necessary to elucidate detailed characteristics of IMC interlayer and the calculation of the thermal stress with that interlayer. In this connection, it will be estimated that the residual stress such as the thermal stress of almost similar joints will be relaxed during the cooling stage of PWHT process because the mechanical and thermal properties are same [51]. However, the thermal stress of dissimilar joint such as the combination in this study was not relaxed during the cooling stage of PWHT process as shown in Figs. 16 through 18. That is, the thermal stress of a dissimilar joint during the cooling stage of PWHT process was generated like as fusion welding [52] due to the difference of mechanical and thermal properties. Therefore, the dissimilar joint subjected to PWHT will be able to consider that it was welded. Hence, the joint between CP-Mg and CP-Al is not suitable for use in high temperature conditions.

5. Conclusions

This report described the investigation of the joint properties of friction welded joint between pure magnesium (CP-Mg) and pure aluminium (CP-Al) with post-weld heat treatment (PWHT). The followings were concluded.

1) The joint in as-welded condition, which was made with a friction speed of 25 s^{-1}, a friction pressure of 50 MPa, a friction time of 1.0 s, and a forge pressure of 90 MPa, had approximately 100% joint efficiency. However, this joint fractured from the adjacent region of the weld interface. In addition, this joint had the intermediate layer (interlayer) consisting of intermetallic compound (IMC) on the weld interface, and its thickness was below approximately 1 μm.
2) Most of joints subjected to PWHT autogenously fractured at IMC interlayer and that mainly occurred between Mg_2Al_3 and $Mg_{17}Al_{12}$ although those layers

had a little each other at the fractured surfaces. That is, this joint was approximately 0% joint efficiency, and the IMC interlayer was composed with mainly Mg_2Al_3 on CP-Mg side and $Mg_{17}Al_{12}$ on CP-Al side.

3) The IMC interlayer grew to CP-Mg and CP-Al sides of the joint, and its thickness increased with increasing heating temperature and/or heating time. Then, the thickness of Mg_2Al_3 was thicker than that of $Mg_{17}Al_{12}$.

4) The thermal stress in the radial and/or circumferential directions of the joint at room temperature after PWHT was larger than that of the axial (longitudinal) direction, and those results were calculated by FEM thermal elastic-plastic analysis.

5) The main reasons for the autogenous fracture from the adjacent region of the weld interface of the joint were considered the growth of IMC interlayer of the joint during PWHT process. Furthermore, that fracture was thought the generating of the thermal stresses in the radial and/or circumferential directions during the cooling stage of PWHT process.

Acknowledgements

The authors wish to thank Mr Hideaki Tohkuni and Mr Harumi Hashimoto in Kitami Institute of Technology for their kindly and aggressive assisting to this study. We also wish to thank the alumnus Mr Norikuni Morikawa, Mr Hideaki Yamane, Mr Yosuke Katsumi, Mr Jun Murayama, and Ms Yukari Anezaki in Kitami Institute of Technology for their devoted contributions to this research project.

References

[1] American Welding Society. Welding handbook. 7th ed. Miami, FL: American Welding Society; 1982. Vol. 4. p. 537-8.

[2] Murti KGK, Sundaresan S. Thermal Behavior of Austenitic-Ferritic Transition Joints Made by Friction Welding. Weld J (supplement) 1985; 64(12): 327s-34s.

[3] Ochi H, Ogawa K, Yamamoto Y, Suga Y. Effect of heat treatment on friction welded joint strength of 6061 aluminum alloy to SUS304 stainless steel. J Japanese Soc Str Frac Mat 1998; 32(2): 43-50 [in Japanese].

[4] Li HY, Huang ZW, Bray S, Baxter G, Browen P. High temperature fatigue of friction welded joints in dissimilar nickel based superalloys. Mater Sci Technol 2007; 23(12): 1408-18.

[5] Feng AH, Xiao BL, Ma ZY. Effect of microstructural evolution on mechanical properties of friction stir welded AA2009/SiCp composite. Compos Sci Tech 2008; 68(9): 2141-8.

[6] Hassan AS, Mahmoud TS, Mahmoud FH, Khalifa TA. Friction stir welding of dissimilar A319 and A356 aluminium cast alloys. Sci Technol Weld Join 2010; 15(5): 414-22.

[7] Krishnan MM, Marimuthu K. Effect of post-weld heat treatment on dissimilar friction stir welded AA6063 and A319 aluminum alloys. Int J Mater Res 2014; 105(5): 507-11.

[8] Mousavi SAAA, Sartangi PF. Effect of post-weld heat treatment on the interface microstructure of explosively welded titanium-stainless steel composite. Mater Sci Eng A 2008; 494: 329-36.

[9] Serizawa H, Mori D, Ogiwara H, Mori H. Effect of laser beam position on mechanical properties of F82H/SUS316L butt-joint welded by fiber laser. Fusion Eng Des 2014; 89(7/8): 1764-8.

[10] Hsieh CT, Chu CY, Shiue RK, Tsay LW. The effect of post-weld heat treatment on the noched tensile fracture of Ti-6Al-4V to Ti-6Al-6V-2Sn dissimilar laser welds. Mater Des 2014; 59: 227-32.

[11] Chu CY, Hsieh CT, Tsay LW. Microstructure and notched tensile fracture of Ti-6Al-4V to Ti-4.5Al-3V-2Fe-2Mo dissimilar welds. Mater Des 2014; 63: 14-9.

[12] Albert SK, Das CR, Sam S, Mastanaish P, Patel M, Bhaduri AK, Jayakumar T, Murthy CVS, Kumar R. Mechanical properties of similar and dissimilar weldments of RAFMS and AISI 316l (N) SS prepared by electron beam welding process. Fusion Eng Des 2014; 89(7/8): 1605-10.

[13] Sarafan S, Wanjara P, Champliaud H, Thibault D. Characteristics of an autogenous single pass electron beam weld in thick gage CA6NM steel. Int J Adv Manuf Tech 2015; 78(9/12): 1523-35.

[14] Bhaduri AK, Rai SK, Gill TPS, Sujith S, Jayakumar T. Evaluation of repair welding procedures for 2.25Cr-1Mo and 9Cr-1Mo steel welds. Sci Technol Weld Join 2001; 6(2): 89-93.

[15] Dong H, Yang L, Dong C, Kou S. Improving arc joining of Al to steel and Al to stainless steel. Mater Sci Eng A 2012; 534; 424-35.

[16] Chen G, Zhang Q, Liu J, Wang J, Yu X, Hua J, Bai X, Zhang T, Zhang J, Tang W. Microstructures and mechanical properties of T92/Super304H dissimilar steel weld joints after high-temperature ageing. Mater Des 2013; 44: 469-75.

[17] Kim YC, Bang HS. The General Conditions Which The Reheat Cracking Test Specimen Must Have. Q J Jpn Weld Soc 2001; 19(1): 148-55 [in Japanese].

[18] Kim YR, Kim JW. A Study on the Thermal Stress Analysis of Thick Plate Structures in Post Weld Heat Treatment. Int J Precis Eng Manuf 2013; 14(2): 247-52.

[19] Fuji A, Ameyama K, North TH. Improved mechanical properties in dissimilar Ti-AISI 304L joints. J Mater Sci 1996; 31(3): 819-27.

[20] Fuji A. *In situ* observation of interlayer growth during heat treatment of friction weld joint between pure titanium and pure aluminium. Sci Technol Weld Join 2002; 7(6): 413-6.

[21] Fuji A, Kimura M, North TH, Ameyama K, Aki M. Mechanical properties of titanium-5083 aluminium alloy friction joints. Mater Sci Technol 1997; 13(8): 673-8.

[22] Fuji A, Horiuchi Y, Yamamoto K. Friction welding

of pure titanium and pure nickel. Sci Technol Weld Join 2005; 10(3): 287-94.
[23] Fuji A. Friction welding of Al-Mg-Si alloy to Ni-Cr-Mo low alloy steel. Sci Technol Weld Join 2004; 9(1): 83-9.
[24] Kimura M, Ishii H, Kusaka M, Kaizu K, Fuji A. Joining phenomena and joint strength of friction welded joint between pure aluminium and low carbon steel. Sci Technol Weld Join 2009; 14(5): 388-95.
[25] Kimura M, Kusaka M, Kaizu K, Fuji A. Effect of post-weld heat treatment on joint properties of friction welded joint between brass and low carbon steel. Sci Technol Weld Join 2010; 15(7): 590-6.
[26] Kimura M, Fuji A, Konno Y, Itoh S, Kim YC. Investigation of fracture for friction welded joint between pure nickel and pure aluminium with post-weld heat treatment. Mater Des 2014; 57: 503-9.
[27] Kimura M, Fuji A, Konno Y, Itoh S. Thermal stress and fracture of friction welded joint between pure Ni and pure Al with post-weld heat treatment. J Fail Anal Preven 2015; 15(2): 300-10.
[28] Kato K, Tokisue H. Mechanical properties and behavior of compound layer on friction welded Mg/Al joints. Preprints of the National Meeting of Jpn Weld Soc 2000; 66: 210-1 [in Japanese].
[29] Morozumi S, Sakurai T, Minegishi T, Kato K, Tokisue H. Strength and structure of the bonding interface in friction-welded 1050 aluminum and AZ31 magnesium alloy joint. J Jpn Inst Light Met 1990; 40(3): 209-14 [in Japanese].
[30] Yasutomi M, Ogawa K, Ochi H, Yamaguchi H, Yamamoto Y, Tsujino R. Evaluation of tensile strength of friction-welded similar joints of AZ31B magnesium alloy and dissimilar joints of AZ31B to 6061 aluminum alloy. J Jpn Soc Str Fracture Mats 2004; 38(2): 29-34 [in Japanese].
[31] Li Y, Liu P, Wang J, Ma H. XRD and SEM analysis near the diffusion bonding interface of Mg/Al Dissimilar materials. Vacuum 2007; 82(1): 15-9.
[32] Morishige T, Kawaguchi A, Tsujikawa M, Hino M, Hirata T, Higashi K. Dissimilar Welding of Al and Mg Alloys by FSW. Mater Trans 2008; 49(5): 1129-31.
[33] Suhuddin UFH, Fischer V, dos Santos JF. The thermal cycle during the dissimilar friction spot welding of aluminum and magnesium alloy. Scr Mater 2013; 68(1): 87-90.
[34] Panteli A, Robson JD, Chen YC, Prangnell PB. The Effectiveness of Surface Coatings on Preventing Interfacial Reaction During Ultrasonic Welding of Aluminum to Magnesium. Metall Mater Trans A 2013; 44(13): 5773-81.
[35] Zhang N, Wang W, Cao X, Wu J. The effect of annealing on the interface microstructure and mechanical characteristics of AZ31B/AA6061 composite plates fabricated by explosive welding. Mater Des 2015; 65: 1100-9.
[36] Liu L, Wang H. Microstructure and Properties Analysis of Laser Welding and Laser Weld Bonding Mg to Al Joints. Metall Mater Trans A 2011; 42(4): 1044-50.
[37] Lee KS, Lee YS, Kwon YN. Influence of secondary warm rolling on the interface microstructure and mechanical properies of a roo-bonded three-ply Al/Mg/Al seet. Mater Sci Eng A 2014; 606: 205-13.
[38] Luo C, Liang W, Chen Z, Zhang J, Chi C, Yang F, Effect of high temperature annealing and subsequent hot rolling on microstructure evolution at the bond-interface of Al/Mg/Al alloy laminated composites. Mater Charact 2013; 84: 34-40.
[39] Saleh H, Reicelt S, Schmidtchen M, Schwarz F, Kawalla R, Krueger L. Effect of inter-metallic phases on the bonding strength and forming properties of Al/Mg sandwiched composite. Key Eng Mater 2014; 622/623: 467-75.
[40] Kim YC, Fuji A, North TH. Characterisation and Production Mechanism of Residual Stress and Plastic Strain in Titanium/AISI304L Stainless Steel Friction Welds. Q J Jpn Weld Soc 1994; 12(2): 243-8 [in Japanese].
[41] Japan Light Metal Association. Aluminium Handbook. 7th ed. Tokyo: Japan Light Metal Association; 2007. p. 36-57 [in Japanese].
[42] The Japan Magnmesium Association. Handbook of Advanced Magnesium Technology. Tokyo: Kallos Publishing; 2000. p. 117 [in Japanese].
[43] The Japan Society for Technology of Plasticity. Magnesium Processing Technology. Tokyo: Corona Publishing; 2004. p. 14-6 [in Japanese].
[44] Kojima Y. Mechanical Properties of Magunesium. The journal of the Surface Finishing Society of Japan 1993; 44(11): 866-73 [in Japanese].
[45] The Japan Magnesium Association. Properties database of Magunesium Materials. Available at: http://metal.matdb.jp/magne/MG02S1101.cfm; 2012. (accessed in October 2012).
[46] Japan Institute of Metals. Metals data book. 4th ed. Tokyo: Maruzen Publishing; 2008. p. 13-4 [in Japanese].
[47] Japan Society of Thermophysical Properties. Thermophysical Properties Handbook. Tokyo: Yokendo; 2008. p 23-6 [in Japanese].
[48] Itoh S, Kameyama M, Mochizuki M. Effects of PWHT on Residual Stress Distribution under Dissimilar Joint. Preprints of the National Meeting of Jpn Weld Soc 2009; 85: 74-5 [in Japanese].
[49] Wang KY, Lu H, Gong L. Evolution of residual stresses in dissimilar steel surfacing layers during process of post-weld heat treatment. Sci Technol Weld Join 2013; 18(3): 210-5.
[50] Terasaki T, Seo K, Hirai T. Dominating Parameters of Residual Stress Distribution. Q J Jpn Weld Soc 1987; 5(4): 533-7 [in Japanese].
[51] Huang CC, Pan YC, Chuang TH. Effects of Post-Weld Heat Treatments on the Residual Stress and Mechanical Properties of Electron Beam

Welded SAE 4130 Steel Plates. J Mater Eng and Perform 1997; 6(1): 61-8.

[52] Abdulaliyev Z, Ataoglu S, Guney D. Thermal Stresses in Butt-Jointed Thick Plates from Different Materials. Weld J (supplement) 2007; 86(7): 201s-4s.